Philosophical Magazine,
Vol. 86, No. 19, 1 July 2006, 2907–2917

Taylor & Francis
Taylor & Francis Group

Radiolytic purification of CaO by electron beams

K. A. MKHOYAN*†, J. SILCOX†,
M. A. MCGUIRE‡ and F. J. DISALVO§

†School of Applied and Engineering Physics, Cornell University,
Ithaca, NY 14853, USA
‡Department of Physics, Cornell University, Ithaca, NY 14853, USA
§Department of Chemistry and Chemical Biology, Cornell University,
Ithaca, NY 14853, USA

(*Received 31 October 2005; in final form 27 February 2006*)

Analysis of the electron energy loss spectra of core-level electronic transitions, O K- and Ca $L_{2,3}$-edges, combined with composition-sensitive annular dark field imaging shows that under electron-beam irradiation portlandite can easily be transformed into calcium oxide. The low-loss region of the energy loss spectra measured before and after transformation also supports the observations. Two possible mechanisms of the electron beam-induced modification of the specimen, radiolysis and knock-on damage, are discussed, and it was found that radiolysis is likely to be the primary mechanism for this transformation of $Ca(OH)_2$ into CaO, while some knock-on damage is also expected.

1. Introduction

Despite the presence of extensive experimental and theoretical research on lime (CaO) [1–3] and portlandite ($Ca(OH)_2$) [4, 5], very little is known about the dynamics of transition from CaO into $Ca(OH)_2$ or from $Ca(OH)_2$ into CaO. Structurally, CaO and $Ca(OH)_2$ are quite different: CaO has a cubic sodium chloride crystal structure with $a_0 = 4.810$ Å, whereas $Ca(OH)_2$ forms a layered hexagonal cadmium hydroxide crystal ($a_0 = 3.584$ Å, $c_0 = 4.896$ Å) [6]. In both crystals, Ca atoms are bonded to six neighbouring O atoms. The O atoms, on the other hand, are bonded to six Ca atoms in CaO and only three Ca and one H atom in $Ca(OH)_2$. This difference in coordination number for oxygen atoms makes them a favourable target for spectroscopic measurements aimed to understand structural modifications. In this paper we present results based on electron energy loss spectroscopy (EELS) indicating that $Ca(OH)_2$ can be purified back into CaO under electron-beam irradiation.

The analytical scanning transmission electron microscope (STEM) is an excellent tool for *in situ* chemical analysis of the specimens. In STEM the analysis can be carried out with a wide range of incident electron beam current densities essential for dose dependent measurements. Electron energy loss spectroscopy coupled with

*Corresponding author. Email: kam55@cornell.edu

Philosophical Magazine
ISSN 1478–6435 print/ISSN 1478–6443 online © 2006 Taylor & Francis
http://www.tandf.co.uk/journals
DOI: 10.1080/14786430600658025

the annular dark field imaging capabilities of STEM allows one to measure local composition of the specimens based on fingerprints of the electronic core-level transitions [7]. These types of measurements can be done on a scale as small as the probe size, which can now reach 0.8 Å in aberration corrected microscopes [8]. The low-loss region of the energy loss spectra (0–50 eV) is also rich with information about physical properties of the material: surface and bulk plasmons, electronic interband transitions, etc. [9, 10].

2. Sample preparation and instrumentation

All specimens studied here were made from original 99.995% CaO chunks obtained from Aldrich Chemical Co. First, small pieces of the CaO were manually crushed in air into powder. Then the powder was washed in isopropanol and very fine particles were suspended on a standard TEM copper grid covered with a holey-carbon-film. After 5–10 minutes of air drying the grid with particles was loaded into the microscope where ultra-high vacuum is maintained. Whereas these manually ground particles had a 10 nm to 10 μm size distribution, the ones picked for study in STEM were 10–40 nm in size and, therefore, transparent to the electron beam. Analytical electron microscopy studies of the particles were carried out on the Cornell 100 kV VG HB-501 STEM. This microscope has a field emission gun, a high resolution pole piece with spherical and chromatic aberration coefficients of $C_s = 1.3$ mm and $C_c \approx 1.5$ mm, and is designed to achieve a 2 Å circular probe with 10–12 mrad incident beam convergent angle (objective angle). The STEM is also equipped with a composition sensitive annular dark field (ADF) detector with 54 mrad inner and 330 mrad outer collection angles and an electron spectrometer for energy loss spectroscopy. During data acquisition for EELS analysis, the microscope was operated with a 20 mrad collection aperture (collection angle). The energy resolution of the spectrometer is 0.5–0.7 eV with an energy drift of $<0.03\,\text{eV}\,\text{min}^{-1}$ over the energy range of 0–2 keV [11].

Powder x-ray diffraction (PXRD) data were collected on a Scintag 2000 theta-theta diffractometer using Cu-K_α radiation ($\lambda_1 = 1.54051$ Å, $\lambda_2 = 1.54433$ Å). Scans from 15 to 70° 2θ at a speed of 0.6 s per step and step size of 0.02° were sufficient for this purpose. Quantitative phase analyses of the PXRD data were performed using the program Fullprof [12].

3. Results

For understanding modifications of the sample that take place under electron-beam irradiation, knowledge of the composition of the initial particles loaded into the microscope is essential. X-ray diffractometry measurements, therefore, were conducted on three different powders. The powders were prepared from as-received CaO chunks by different treatments: (i) manually ground using an agate mortar and pestle, (ii) ball-milled with agate balls in an agate vial, and finally, (iii) manually

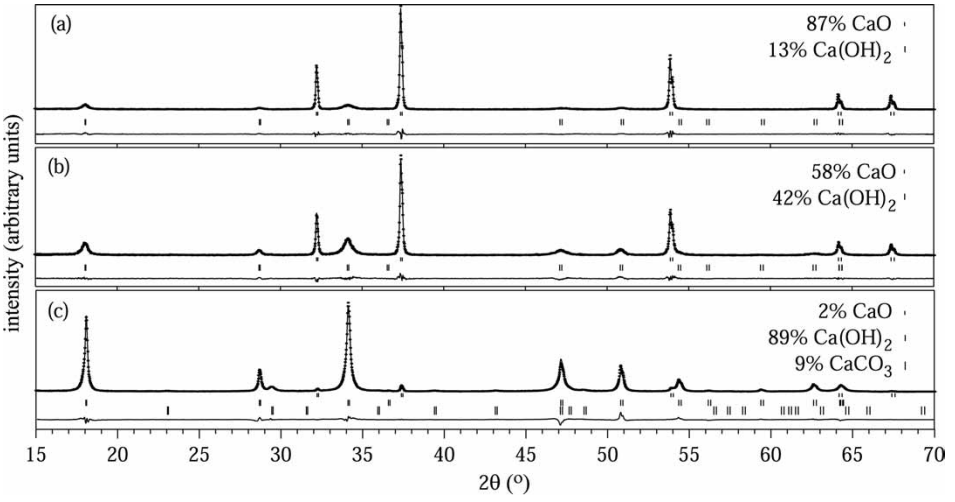

Figure 1. Rietveld refinements of the PXRD patterns for (a) CaO ground with an agate mortar and pestle, (b) CaO ball-milled for five minutes and (c) CaO powder from (a) washed in isopropanol. The powder in (c) was scanned with a speed of 6 s per step for better S/N ratio. Here the circles represent the measured data and the lines are the calculated patterns. Tick marks indicate the positions of the Bragg reflections for each phase. The difference curves between the measured data and theoretical fits are also presented at the bottom of each panel. Each pattern is labelled with the weight percent of CaO, $Ca(OH)_2$ and $CaCO_3$ present in the sample.

ground and isopropanol washed. All three powders were prepared in air. The results of the PXRD scans are presented in figure 1. As was expected, CaO powders exposed to the air absorb water and transform into $Ca(OH)_2$. The results of phase analysis indicate that for manually ground powder the percentage of the $Ca(OH)_2$ is 13% (all the percentages in the paper are at.%), whereas for fine ball-milled powder it is 42%. Not surprisingly, the smaller the particles are, the more surface area is exposed to air, and consequently a higher percentage of the $Ca(OH)_2$ is in the powder. It should be noted here that the amount of the CaO transformed into $Ca(OH)_2$ in air is also a function of time and for sufficiently long times all CaO will transform into $Ca(OH)_2$ and eventually into $CaCO_3$. The measurements conducted on powder (iii) show that after washing in isopropanol practically all CaO is transformed into $Ca(OH)_2$ (see figure 1c). This is likely due to a reaction of the CaO with a small amount of water present in the isopropanol. A small percentage of $CaCO_3$ also observed in the measurement is a result of further reactions of $Ca(OH)_2$ with CO_2 present in the air. The results of the PXRD measurements indicate that the majority (90%) of the particles loaded in the STEM (corresponding to the case (iii)) are $Ca(OH)_2$ demonstrating the importance of detailed characterization of air sensitive specimens prior to any microscopy study. However, since the particles loaded in STEM were exposed only 5–10 minutes to air after the isopropanol wash, less than 9% of calcium carbonate is expected to be present.

The STEM measurements on these specimens revealed two critical observations. First, with an incident beam current of 15 pA, the specimens experience rapid

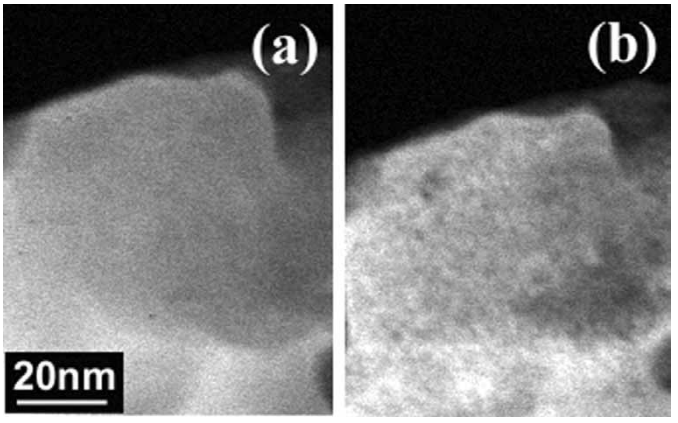

Figure 2. ADF images of the specimen recorded before and after electron-beam-irradiation. An electron dose of $30\,C\,cm^{-2}$ was used for this transformation.

modification within a few seconds, and second, after modification the new substance remains unaffected by the beam. An electron beam dose of $20\,C\,cm^{-2}$ was sufficient to completely modify $4 \times 10^4\,nm^3$ portlandite into something new, which, as we will see later, is pure CaO. ADF images of the specimen recorded before and after transformation, after exposing it to a $30\,C\,cm^{-2}$ electron dose, are presented in figure 2. Changes of surface morphology and size reduction are characteristic features that occur with transformation.

For determination of the composition of the substance at every stage of transformation, EELS analysis was carried out. Spectra of oxygen K- and calcium $L_{2,3}$-edges were recorded before, during and after transformation. The results, after background subtraction using the standard $f(E) = AE^{-r}$ fit [10], are presented in figure 3. In these measurements the beam current density was reduced to $0.4\,A\,cm^{-2}$, to allow monitoring the transformation without causing significant changes during acquisition of a single spectrum (3 s acquisition was used for recording each EELS spectrum). As can be seen from figure 3a the dominating peak of the O K-edge at 539.7 eV in $Ca(OH)_2$ decreases significantly with electron-beam irradiation, while the peak at 534.0 eV, characteristic of CaO, becomes more and more pronounced. The spectrum of the O K-edge recorded after completion of the transformation displays all the details of the characteristic O K-edge in CaO [13, 14]. These suggest that transformation of the specimen under electron-beam irradiation is actually CaO purification. We should note here that due to a higher energy resolution of the Cornell STEM more details of the O K-edge fine structure were revealed in these measurements than those reported in literature [13, 14].

Earlier studies of CaO show that multiple scattering (MS) [15] is an excellent method for calculating and identifying the features in the fine structure of some core-edges observed by X-ray absorption [16, 17]. In many ways EELS and X-ray absorption spectroscopy (XAS) are similar. In both cases, in the inelastic scattering event (in one case with an incident energetic electron, and in other with an incident photon) one of the electrons in the core state of an atom in the

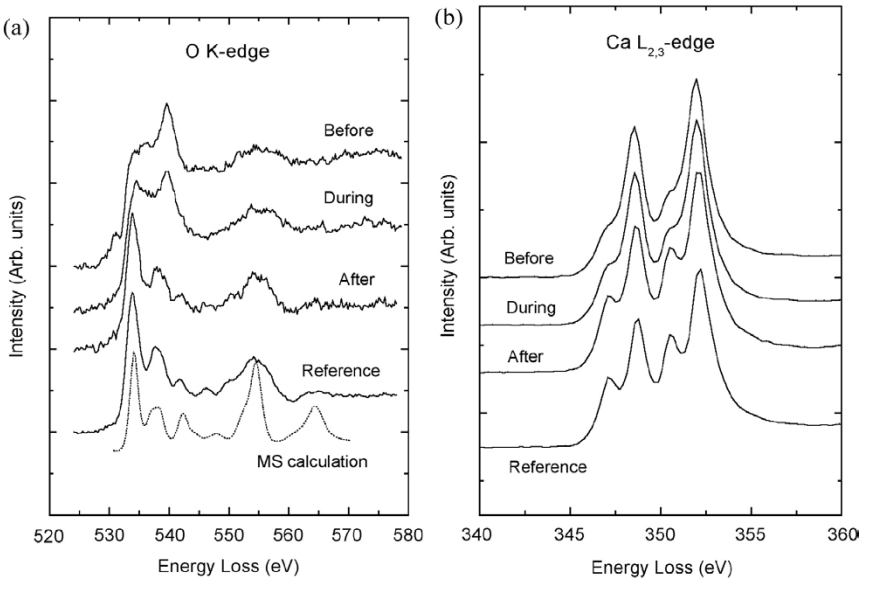

Figure 3. EELS data recorded before, during and after transformation. (a) Core-loss spectra of the O K-edge. (b) Spectra of the Ca $L_{2,3}$-edge. In both graphs (a, b) the spectra labelled 'Reference' are the spectra of the final and stable substance recorded with a better S/N ratio. Curve labelled 'MS calculation' in (a) is a simulated spectrum of the O K-edge in CaO calculated using the multiple scattering method.

specimen is transferred into the empty states of the band structure of the solid. In the small scattering angle approximation the matrix elements of EELS and XAS are very similar (see, for example, Egerton [10] or section 4.1 of Stöhr [18]), suggesting that the MS calculation can also be used to understand details of the fine structure in the core-level EELS. The MS calculation of the O K-edge in the CaO was conducted using the FDMNES code of Joly [19]. The results of these calculations, where a muffin-tin approximation for the crystal potential and a Green's function formalism for multiple scattering were used, are presented in figure 3a. In these calculations a 10% overlap between the spheres of the muffin-tin potential was applied and acceptable convergence was reached with the inclusion of 93 neighbouring atoms. Good agreement between the MS calculation and EELS data confirms the presence of all the peaks resolved in our measurement.

EELS measurements of the Ca $L_{2,3}$-edge, presented in figure 3b, also show detectable modifications in fine structure with electron-beam-irradiation. Two bumps at around 347 and 351 eV in $Ca(OH)_2$ after transformation become well defined peaks at 347.1 and 350.5 eV correspondingly. Since the environments of the Ca atoms are similar in CaO and $Ca(OH)_2$, little difference was expected in Ca $L_{2,3}$-edge spectra of the two compounds. It should be noted here that no shift in energy was observed between the peaks of Ca $L_{2,3}$-edge before and after transformation. Comparison of the Ca $L_{2,3}$-edge recorded after modification with

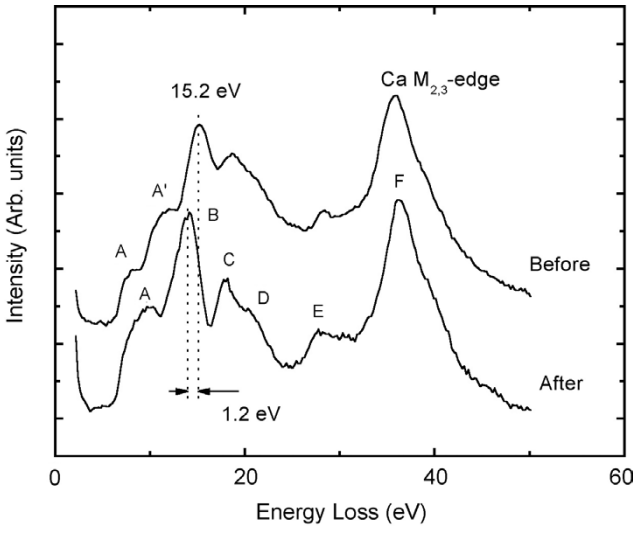

Figure 4. Low-loss region of EELS. The spectra were recorded before and after transformation. All resolvable peaks are labelled A to F and their positions are presented in table 1.

corresponding data from CaO reported by Saldatov *et al.* [17] and Himpsel *et al.* [20] confirms that the final substance created in the STEM with electron beam irradiation is indeed CaO.

The low-loss regions of the EELS spectra were also recorded before and after transformation. The results are presented in figure 4. A shift in bulk plasmon energy from 15.2 eV for $Ca(OH)_2$ to 14.0 eV and the conversion of the two peaks A and A′ into a single peak at 10.0 eV are the major modifications. No visible changes were observed in the 30–50 eV energy range, where the dominating feature is the core-loss spectra of the Ca $M_{2,3}$-edge [10, 21]. In the reports by Protheroe *et al.* [22] and Waltenburg and Moller [23] the low-loss EELS spectra for CaO are presented and origins of the major peaks are discussed. The spectrum of the low-loss EELS recorded here after transformation is in excellent agreement in general shape and position of the peaks presented in those reports. The positions of the major peaks in $Ca(OH)_2$ and CaO are listed in table 1. Due to slight differences in the location of the peaks in the earlier studies [22, 23], a comparison of our measurement with the two former results is also made in the same table. It appears that the results of this work are in better agreement those of Waltenburg and Moller [23].

As was mentioned earlier the second critical observation was the stability of the CaO formed after electron-beam-irradiation. To confirm those initial observations, several spectra of the O K- and Ca $L_{2,3}$-edges were recorded again, but now with 10 s exposure times. In these measurements the electron beam current density was increased by 100 to enhance the possible effects. The results, presented in figure 5, show no visible changes in fine structure of either the O K- or the Ca $L_{2,3}$-edge even after extensive electron-beam irradiation.

Table 1. Position of the peaks in the low-loss region of EELS and comparison with data reported by Waltenburg and Moller [23] and Protheroe *et al*. [22]. For the identification of the peaks labelled A–F see figure 4.

	Energy loss (eV)			
	This work		[23]	[22]
Peak	$Ca(OH)_2$	CaO	CaO	CaO
A	8.3	10.0	10.0	9.15 ± 0.05
A′	12.2	–	–	–
B	15.2	14.0	14.2	13.1 ± 0.1
C	18.7	18.0	18.5	17.3 ± 0.1
D	–	20.1	–	20.3 ± 0.1
E	28.4	28.1	28.5	27.4 ± 0.1
F	36.2	36.2	36.4	35.0 ± 0.2

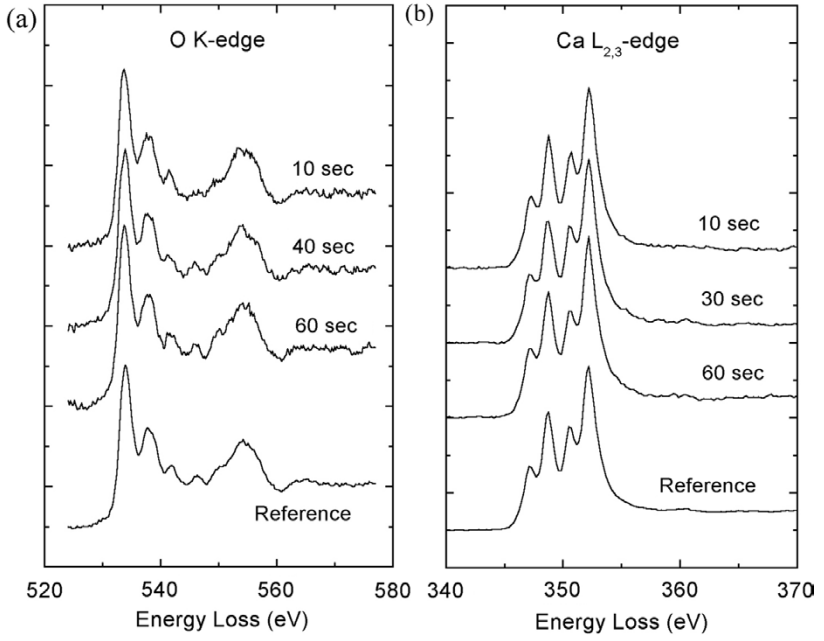

Figure 5. EELS spectra of O K- and Ca $L_{2,3}$-edges recorded from the CaO with progressively increasing exposure times. In these measurements the beam current density was increased by 100.

4. Discussion

EELS measurements of the O K- and Ca $L_{2,3}$-edges as well as low-loss spectra clearly show that $Ca(OH)_2$ can be easily transformed into CaO by electron-beam irradiation. The reaction

$$Ca(OH)_2(s) \rightarrow CaO(s) + H_2O(g) \quad (1)$$

should be thermodynamically favourable when the Gibbs free energy change for the reaction ΔG is less than or equal to zero:

$$\Delta G = \Delta G^0 + k_B T \ln P_w \leq 0. \tag{2}$$

Here ΔG^0 is the free energy of the reaction at standard conditions ($T = 298\,\mathrm{K}$, $P_w = 1\,\mathrm{atm}$), k_B is the Boltzmann constant, T is the absolute temperature and P_w is the water vapour pressure (in atm). From standard tables of free energies of formation [24], $\Delta G^0 = 65.8\,\mathrm{kJ\,mol^{-1}}$. Equation (2) is strictly true only for $T = 298\,\mathrm{K}$ and a small correction must be made to account for variation in temperature. Thus, we must consider the heating of the sample due to electron-beam irradiation. In transmission electron microscopes, significant temperature rise, including the melting of particles due to heating under electron-beam irradiation, has been reported previously [25–27].

The temperature increase in the exposure area can be estimated using the Bethe expression for mean energy loss per unit path of the incident electron [27, 28]. Using the small-area illumination approximation, where the dimensions of the irradiated area are considered to be much smaller than dimensions of the specimen ($r_0 \ll R$), the temperature rise in the irradiated area can be described as [27]:

$$\Delta T = \frac{j\rho}{2e\lambda}\left[\frac{e^4 N_A Z}{4\pi\varepsilon_0^2 A E_0 \beta^2}\ln\left(\frac{E_0\beta^2}{2J}\right)\right] r_0^2 \ln\left(\frac{R}{r_0}\right) \tag{3}$$

where j is the irradiation current density, ρ, λ and Z are the density, thermal conductivity and average atomic number of the specimen, E_0 is the energy of incident electrons and $J \approx 13.5Z$ is the mean ionization energy. Under the conditions of experiments conducted in this study (parameters for $Ca(OH)_2$ and CaO can be found in Lide [24]), according to equation (3), the temperature in the irradiated area can not increase more than a few degrees ($<2^\circ$C). Thus to a good approximation we can assume the temperature of the sample is constant, and equation (2) holds.

The magnitude of the partial water vapour pressure that is necessary for reaction (1) to take place was estimated using equation (2). After substituting the values for the free energies [24] and temperature it can be shown that a pressure less than 3×10^{-9} Torr is needed for the reaction (1) to be thermodynamically favourable in the chamber of the microscope. The partial pressure for the water vapour in the column of the microscope, measured using a VG Anavac residual gas analyzer mounted on a port on the specimen chamber, was recorded to be $\approx 6 \times 10^{-9}$ Torr (with total pressure of $\approx 2 \times 10^{-8}$ Torr). We should note that at the same time the pressure of specimen chamber, when measured by the standard ion-gauge mounted in the pumping line, was 5×10^{-10} Torr indicating an order of magnitude better vacuum in the pumping line than in the actual specimen chamber. The pressure inside the pole-piece of the objective lens, in the area near to the specimen where pumping is not as efficient as in the column, is expected to be in the region of 10^{-8} Torr. These measurements suggest that reaction (1) can not occur spontaneously and substantial incident electron beam–specimen interaction should be in play.

Two primary mechanisms for the alteration of the specimen during TEM observations due to the interaction of fast incident electrons of the probe with the atoms of the specimens are knock-on damage and radiolysis [29]. During knock-on damage an incident energetic electron of the probe in a direct collision transfers a significant amount of energy to the atoms of the specimen. If the binding of the atom in the crystal is not strong then this transferred energy can be sufficient to remove an atom from its site or sputter it from the surface [30, 31]. The maximum energy that can be transferred to the atom in a collision can be estimated using the equation [27]

$$E_{\max} = \frac{2E_0\left(E_0 + 2m_0c^2\right)}{M_0c^2} \tag{4}$$

where M_0 is the mass of the atom. In table 2, the maximum energies that can be transferred to Ca, O and H in direct collisions with 100 keV electrons are listed. In the same table we present also the binding energies of these atoms in $Ca(OH)_2$ and CaO.

The probabilities for surface sputtering and vacancy enhanced displacement, which are the dominating processes for knock-on damage, can be described using Mott cross-sections [32–35]. Since the cross-sections for surface sputtering and vacancy enhanced displacement are similar, in table 2 we listed only the values for surface sputtering energies and corresponding Mott cross-sections for all atoms in $Ca(OH)_2$ and CaO. Calculations for the reduction of the number of atoms, based on knock-on damage theory developed by Medlin and Howitt [36] and successfully applied to wurtzite InN [31], suggest that for $Ca(OH)_2$ irradiated by 100 keV electrons with dose of $20\,C\,cm^{-2}$ no damage should be expected. It cannot be expected in CaO as well, where the probability of oxygen sputtering is even lower. However, for transformation of the $Ca(OH)_2$ into CaO it is essential to have desorption of the oxygen and hydrogen.

Radiolysis provides atomic displacements in the solid by converting excitonic energies, which are generated after incident probe electron-atomic electron interactions, into momentum by forming a Frankel pair [29]. For radiolysis to take place with any efficiency, two critical requirements should be met: the energy stored in excitons should be at least as large as the energy necessary for atomic

Table 2. List of maximum energies, $E_{\max}$, that can be transferred to Ca, O and H atoms in collision with 100 keV electrons, binding energies (BE), surface sputtering energies (SSE) and Mott cross-sections (M-CS) for each type of atom in $Ca(OH)_2$ and CaO. The numbers for BE were deduced from values in the literature [37–39]. (All energies are in eV).

		Ca	O	H
$E_{\max}$		6.0	15.0	239.5
BE (per O-X bond)	$Ca(OH)_2$	1.9	–	4.9
	CaO	1.8	–	–
SSE	$Ca(OH)_2$	5.7–9.5	5.7	4.9
	CaO	9.0	9.0	–
M-CS (in barns)	$Ca(OH)_2$	–	168.0	89.8
	CaO	–	64.2	–

displacement and relaxation time for excitons should be long enough that mechanical relaxation of the atoms can lead to bonding instabilities. As a result, radiolysis is primarily observed in insulating solids including ice and $CaCO_3$ [29]. The presence of hydrogen in $Ca(OH)_2$ provides critical pathways for localization of the exciton as well as weakens the binding energy for oxygen atoms (see table 2). As in alkali halides with hydrogen impurities [29], hydrogen atoms in $Ca(OH)_2$ can be relocated from their sites by ionization and stimulate radiolysis. In CaO, on the other hand, like in MgO, extremely large displacement energies for Ca and O atoms in the crystal ($\sim$50 eV) (compare to energies stored in excitons ($\sim$25 eV)) make radiolysis unlikely [40].

5. Conclusion

In conclusion, based on EELS analysis of the core-level electronic transition, O K- and Ca $L_{2,3}$-edges, and low-loss EELS it was shown that using electron-beam irradiation portlandite can be easily transformed into calcium oxide. Detailed examination of the possible effects of two mechanisms of the electron beam induced modification of the specimen, radiolysis and knock-on damage, suggests that modification of the $Ca(OH)_2$ into CaO is primarily governed by radiolysis while some knock-on damage is also expected. It was also observed that, unlike $Ca(OH)_2$, CaO is stable under electron beam irradiation. Analysis shows that since knock-on damage is the only possible source for modification of CaO, it is essential to have electron beam doses at least of the order of 20–30 $kC\,cm^{-2}$ to achieve noticeable alterations in the structure.

Acknowledgments

This work is supported primarily by the Nanoscale Science and Engineering Initiative of the NSF EEC-0117770 and NYSTAR C020071. The sample preparation facilities and STEM are supported by NSF through the Cornell Center of Materials Research DMR 9632275. We would also like to acknowledge M. Thomas and E. Kirkland for technical support and S. Maccagnano for critical reading of the manuscript.

References

[1] N. Daude, C. Jouanin and C. Gout, Phys. Rev. B **15** 2399 (1977).
[2] R. Jeanoz, T.J. Ahrens, H.K. Mao, *et al.*, Science **206** 829 (1979).
[3] H. Baltache, R. Khenata, M. Sahnoun, *et al.*, Physica B **344** 334 (2004).
[4] R. Laser and R.G. Gordon, Phys. Rev. B **25** 7221 (1982).
[5] P. Baranek, A. Lichanot, R. Orlando, *et al.*, Chem. Phys. Lett. **340** 362 (2001).
[6] R.W.G. Wyckoff, *Crystal Structures* (Wiley, New York, 1963).
[7] D.A. Muller, D.J. Singh and J. Silcox, Phys. Rev. B **57** 8181 (1998).
[8] P.E. Batson, O.L. Krivanek and N. Dellby, Nature **418** 617 (2002).

[9] P. Batson and J. Silcox, Phys. Rev. B **27** 5224 (1983).
[10] R.F. Egerton, *Electron Energy Loss Spectroscopy in the Electron Microscope* (Plenum, New York, 1996).
[11] K.A. Mkhoyan, Ph.D. Thesis, Cornell University (2004).
[12] J. Rodriguez-Carvajal, *Fullprof 2k, Version 3.30 - June 2005* (LLB, CEA/Saclay, 2005).
[13] X. Weng and P. Rez, Phys. Rev. B **39** 7405 (1989).
[14] H. Gu and M. Ceh, Ultramicroscopy **78** 221 (1999).
[15] J.J. Rehr and R.C. Alers, Rev. Mod. Phys. **72** 621 (2000).
[16] D. Norman, K.B. Garg and P.J. Durham, Solid St. Commun. **56** 895 (1985).
[17] A.V. Saldatov, T.S. Ivanchenko, S.D. Longa, *et al*., Phys. Stat. Sol. (b) **168** K43 (1991).
[18] J. Stöhr, *NEXAFS Spectroscopy* (Springer, Berlin, 1996).
[19] Y. Joly, Phys. Rev. B **63** 125120 (2001).
[20] F.J. Himpsel, U.O. Karlsson, A.B. McLean, *et al*., Phys. Rev. B **43** 6899 (1991).
[21] C.C. Ahn and O.L. Krivanek, *EELS Atlas* (Gatan Inc, 1983).
[22] A.R. Protheroe, A. Steinbrunn and T.E. Gallon, J. Phys. C **15** 4951 (1982).
[23] H.N. Waltenburg and P.J. Moller, Surf. Sci. **439** 139 (1999).
[24] D.R. Lide (Editor), *CRC Handbook of Chemistry and Physics*, 85th edn (Plenum, New York, 2004).
[25] B. Gale and K.F. Hale, Br. J. Appl. Phys. **73,** 5257 (1993).
[26] T. Yokota, M. Murayama and J.M. Howe, Phys. Rev. Lett **91** 265504 (2003).
[27] L. Reimer, *Transmission Electron Microscopy*, Springer Series in Optical Sciences, Vol. 36 (Springer-Verlag, Berlin, 1993).
[28] H. Bethe, Ann. Phys. (Leipzig) **5** 325 (1930).
[29] L.W. Hobbs, in *Introduction to Analytical Electron Microscopy*, edited by J.J. Hren, *et al*. (Plenum, New York, 1979).
[30] D.L. Medlin, L.E. Thomas and D.G. Howitt, Ultramicroscopy **29** 228 (1989).
[31] K.A. Mkhoyan and J. Silcox, Appl. Phys. Lett. **82** 859 (2003).
[32] N.F. Mott, Proc. R. Soc. A **124** 426 (1929).
[33] N.F. Mott, Proc. R. Soc. A **135** 429 (1932).
[34] H. Feshbach, Phys. Rev. **103** 1597 (1956).
[35] C.R. Bradley, *Calculations of Atomic Sputtering and Displacement Cross-Sections in Solid Elements by Electrons with Energies from Threshold to 1.5 MeV*, Report No. ANL-88-48, 1988.
[36] D.L. Medlin and D.G. Howitt, Phil. Mag. Lett. **64** 133 (1991).
[37] P. Baranek, A. Lichanot, R. Orlando, *et al*., Chem. Phys. Lett. **340** 362 (2001).
[38] P. Cortona and A.V. Monteleone, J. Phys. Condensed Matter **8** 8983 (1996).
[39] M. Springborg and O.E. Taurian, J. Phys. C **19** 6347 (1986).
[40] D. Pooley, in *Radiation Damage Processes in Materials*, edited by C.H.S. Dupuy (Hoordhoff, Leyden, 1975).